Tribological Investigations Using Friction Force Microscopy

R. Overney and E. Meyer

Introduction

Many attempts have been made in recent centuries to investigate friction, adhesion, lubrication, and wear. Most of the experimental approaches and theories were based on macroscopic experiments, such as tensile and indentation tests. For a long time, only the bulk properties of the materials were considered.

Late in this century a new term was created combining all of the above-mentioned properties which deal with the science of interacting material interfaces in relative motion: *tribology*. The state of the art of science today reveals that processing in nature depends strongly on interfaces that cannot be described only by bulk properties. Tribologists realize they must study the sliding surfaces by analytical surface-science tools. With the surface force apparatus developed by J.N. Israelachvili and D. Tabor,[40] we have a surface analysis tool that provides new insight into the field of macroscopic sliding contact of lubricated systems.

After Amontons' laws were established[41] as a first attempt to describe sliding friction analytically, theories were advanced over the course of this century. A classic discipline was developed: *contact mechanics*. More quantitative treatments of friction were developed by various authors. The energy dissipation in most processes in tribology induced the theorists to consider the sliding bodies as spring models creating phonon-phonon interactions. And with modern computer facilities, they started to perform computational experiments whenever classical experiments could not provide information on the submicron scale.

With the inception of the field of scanning force microscopies by G. Binnig, C.F. Quate, and C. Gerber[1] in 1986, a surface analysis technique was introduced, able to probe any surface with a resolution on the atomic scale. Many groups worldwide have used this new technique to investigate surfaces of crystalline and amorphous materials and to examine inorganic and organic systems.[2] The design of this real-space analytical tool is based on the scanning tunneling microscope[3] (G. Binnig, H. Rohrer, Nobel Prize, 1986), which scans a very fine tip over the sample surface. The scanning force microscope tip is located on a sensitive cantilever spring. Interactions between the tip and sample cause deflections of the cantilever. These deflections are monitored by a computer providing a two-dimensional image of the sample surface in real space. Depending on the load of the spring, the tip can adhere to the sample and undergo sliding start-up effects, known in tribology as *static friction*, and dynamic sliding effects by scanning. C.M. Mate and G.M. McClelland took advantage of this situation, modified the scanning force microscope, and measured the lateral instead of the normal movement of the tip.[4] Their experiment provided the first friction measurements on the atomic scale.

With the development of the laser beam-deflection method (see next section), G. Meyer et al.[5] and O. Marti et al.[6] produced a single detection setup capable of providing simultaneous information on normal and lateral movement of the tiny cantilever sliding over the sample surface. This article seeks to:

- highlight the problems of crosstalk on the topography and torsion signals and present a method that allows one to distinguish between topographically induced and frictionally induced torsion (*friction loop*), and
- describe the first successful applications of the friction force microscope carried out on lubricating systems, such as organic films, also known as boundary lubricants.

These boundary lubricant films are either physically or chemically adsorbed on the solid surfaces and their exact microscopic nature remains largely unknown. Self-assembled organic films, such as Langmuir-Blodgett (LB) films, serve as model boundary lubricants. These films are known lubricants, behave in a solidlike manner, adhere well to substrates, and form ordered two-dimensional structures. The scanning force microscope provides a unique opportunity to study friction and wear resulting from a microscopic asperity on these organic compounds.

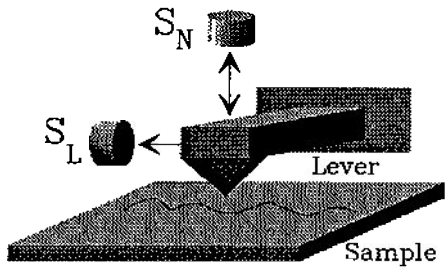

Figure 1. Bidirectional AFM Method (A). Normal and lateral bending is measured by two sensors: S_N (normal) and S_L (lateral). Typically, the feedback control holds the normal force constant. In the setup of Mate et al.,[4] only the lateral sensor is used.

Experimental Details

Mate et al.[4] modified the atomic force microscope (AFM) to measure the deflection of the cantilever in response to *lateral forces* (Figure 1). The sideways bending of the cantilever (tungsten wire) was detected using a laterally positioned optical interferometer. With these early measurements of lateral friction forces, it was demonstrated that it is possible to measure lateral forces on a subnanometer scale on graphite[4] and mica[7] (even though the spring constant of the tungsten wire was 2,500 N/m and 100 N/m, respectively). This astonishing resolution was possible because of the sensitive optical sensor (resolution <0.01 nm). Since those initial experiments, several groups[8-11] have combined normal and lateral-force detection.

Combined normal and lateral-force measurements can be performed by two different methods:

(A) bidirectional measurements with two sensors, and

(B) bidirectional measurements with one sensor.

Method (A) logically extends the normal force measurement by bringing a second, additional sensor (S_L) up sideways to the cantilever (Figure 1). This approach has been implemented by G. McClelland et al.[9] with a two-fiber optical interference ultrahigh vacuum (UHV) AFM, by G. Neubauer et al.[8] with bidirectional capacitance sensor, and in our group with two tunneling detection schemes.[12]

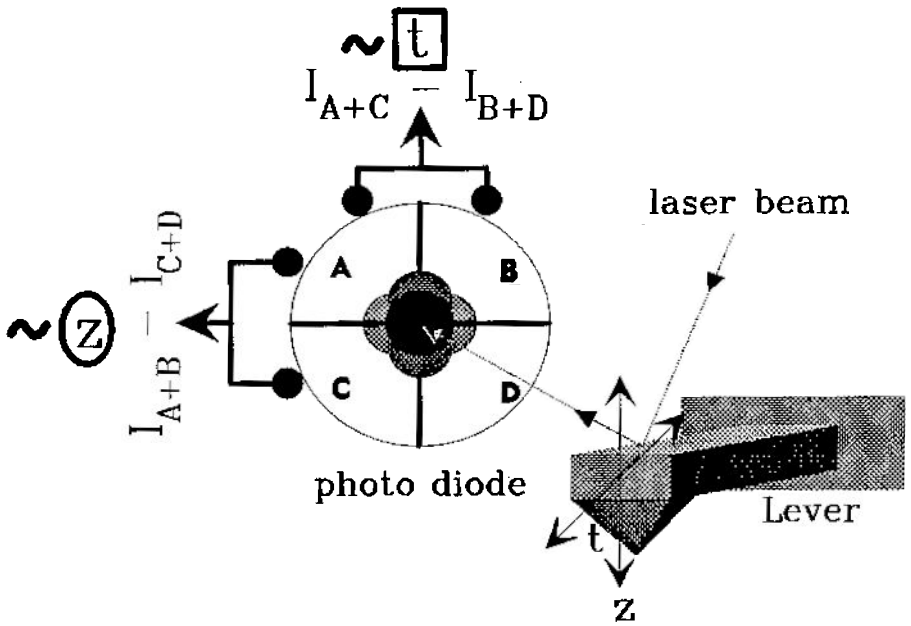

Figure 2. Principle of simultaneous measurement of normal and lateral (torsional) forces. The intensity difference of the upper and lower segments of the photodiode is proportional to the z-bending of the cantilever. The intensity difference between the right and left segments is proportional to the torsion, t, of the force sensor.

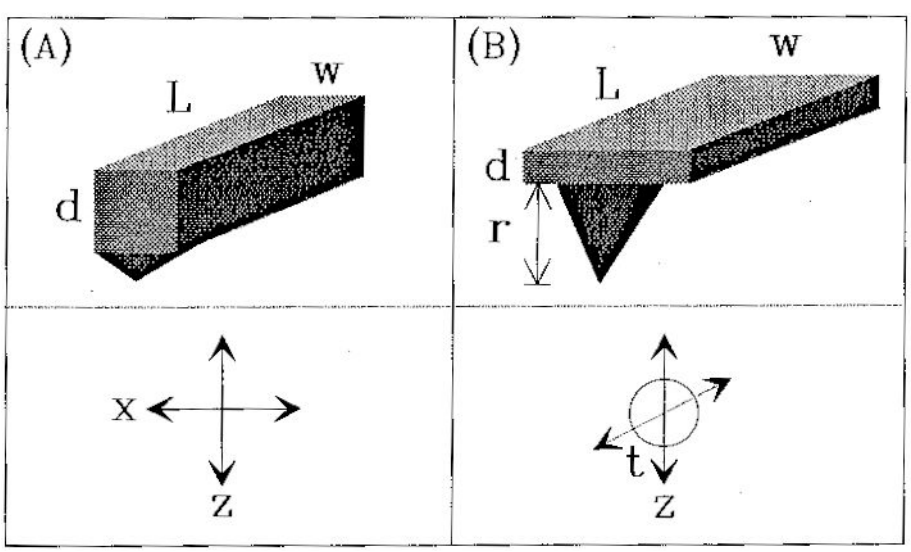

Figure 3. Cross section of cantilevers for methods (A) and (B): (A): x- and z-deflection are measured; (B): z-deflection and torsion, t, are measured.

In measuring the normal deflection simultaneously with the torsion (method B[10,11]), only one sensor is required to acquire lateral (torsional) and normal force information. The reflected beam is monitored with a four-quadrant photo diode (Figure 2). Normal bending of the cantilever is measured by the intensity difference ($I_{A+B} - I_{C+D}$) of the upper and lower segments of the diode. The signal difference ($I_{A+C} - I_{B+D}$) of the left and right segments provides torsional information. These two measurements are performed simultaneously (Figure 2). Within certain limits (see next section), methods (A) and (B) are both sensitive to lateral (frictional) forces. To increase this sensitivity, detection-sensor-specific cantilever shapes are required (Figure 3).

A square or circular cross section of the cantilever is required for method (A), to enable positioning of a second sensor. For method (B), a flat rectangular cross section of the lever is required. Also, a long tip is required for method (B), whereas (A) should have a short one. The reasons for these requirements originate in the formal expression of the spring constants of a rectangular beam (Tables I and II).

Method (B) has the advantage of needing only one detection sensor, and of being convenient in air because the sensor responds quickly to the motion of the lever. In general, with the laser beam deflection scheme, no feedthroughs are required, as in the optical interference AFM, making the method particularly adaptable to a UHV system.[16]

Frictional Information

The aim in measuring lateral or torsional deflections of the cantilever is to receive information about the frictional behavior of the scanned sample with respect to the cantilever tip. In all the detection methods discussed, the deflection sensor position is fixed. This immobilization of the sensor with respect to the dynamics of the cantilever can cause mechanical crosstalk between torsional, lateral, and normal movements. It is irrelevant whether the lateral forces are measured by bending or torsion, as long as the cross section of the cantilever is accommodated in the detection method (cf. Figure 3). The following discussion in lateral-force measurement, therefore, will be based on a sideways-positioned sensor S_L.

As long as the cantilever is gliding over an atomically flat surface, the bending force F_M in the gliding direction scales with the same magnitude as the friction force F_F. The measured lateral bending direction

Table I: Spring Constant Formulas for a Rectangular Beam.[13]

z-bending	$c_z = \frac{Ewd^3}{4L^3}$
x-bending	$c_x = \frac{Ew^3d}{4L^3}$
torsion	$c_t = \frac{Gwd^3}{3Lr^2}$

E = Young's modulus
w = lever width
d = lever thickness
L = lever length
r = tip length
σ = poisson ratio

With the shear modulus:

$$G = \frac{E}{2(1+\sigma)}$$

Table II: Representative Spring Constants for Various Cantilever Configurations (Dimensions).

Cantilever Dimensions	Spring Constants*		
	Si_3N_4[14]		
($L \times w \times d$) [μm]	c_z [N/m]	c_x [N/m]	c_t [Nm]
100 × 10 × 0.6	0.21	58	114
100 × 20 × 0.6	0.41	462	228
200 × 20 × 0.6	0.05	58	114
		Si[15]	
200 × 21 × 0.4	0.007	19	0.72

*Values for Si_3N_4[15] cantilevers are based on $E = 3.85 \times 10^{11}$ Pa,[16] $G = 1.4 \times 10^{11}$ N/m^2,[24] and a tip radius (r) of 3 μm. Values for Si[15,17] cantilevers are based on $E = 1.65 \times 10^{11}$ Pa,[16] $G = 0.5 \times 10^{11}$Pa,[16] $G = 0.5 \times 10^{11}$ N/m^2,[16] and a tip radius (r) of 12.5 μm.

is equal to the lateral movement of the lever. In this case, the detector S_L acts as a tool to monitor real lateral (frictional) forces (Figure 4a).

Scanning over step sites gives rise to high torques on the cantilever tip. This, in turn, alters the cantilever's gliding direction, and the static-positioned sensor no longer measures parallel to the gliding direction (Figure 4b).

It would be possible to recalculate the lateral force F_F if the exact geometry of the cantilever tip were known. In practice, however, the tip geometry and its exact orientation to the sample surface are unknown. Because of the intrinsic problem of a static deflection sensor, frictional measurements, which require force monitoring parallel to the gliding direction, cannot be accurately performed on step sites. Instead, indication of the sharpness (steepness) of the step is deducted from the degree of cantilever twisting.

In order to extract frictional information from the torsion, it is important to compare the *friction loop* (forward and reverse scan of the torsional signal) with the topography. In Figure 5, a forward and reverse scan line of a stepped surface is schematically drawn. The sample surface is assumed to be composed of a homogeneous material except for the lowest surface (e.g., an underlying substrate). Step heights and widths of the terraces can be measured in the topographical mode. At step sites the torsion t shows outlines as discussed above. In the homogeneous part (2), t remains constant on either side of steps. On part (3), where the material is different, the amount of t changes to another constant value. The difference $\Delta t \equiv t_1 - t_3$ is independent of the topography and is material specific. Because the cantilever is sliding, Δt is a measure for the relative *sliding friction* ΔF_{SL}. *Static friction* F_{ST} is given at the beginning (1) and (4) of each forward and reverse scan. The resistance against the sliding direction causes the hysteresis of the *friction loop*, which compares the forward with the reverse scan. The inverse torsional signals of the forward and reverse scan is an important indicating device for deciding whether a torsional feature is caused by topography or friction.

Wear Properties of Organic Lubricants

In the science of tribology, self-assembled organic films play an important part in fluid lubrication.[19] Several studies have demonstrated that the AFM can provide an important new view of ultrathin, well-ordered organic multilayer films.[2,20,21] With small loadings, on the order of 10^{-9}–10^{-8} N, it has been shown to be possible to image Langmuir-Blodgett films.[22,23] Film thickness, mono- and multilayer steps, and the arrangement of molecules in the surface of the film have been recorded.[24–27] The AFM has also been used as a tool to intentionally deform the films, creating features of tailored dimensions. The forces required to deform the films are on the order of 10^{-6} N. More important for achieving plastic deformation than the normal load are intrinsic properties of the film (e.g., packing density), feedback loop frequency, and scan velocity. Wear occurs if the feedback loop frequency is smaller than some critical value, i.e., when the applied shear stress overcomes the material-specific yield point (see Figure 6).

To decrease the feedback control frequency per scan line, the scan velocity and/or the scan area (under constant scan-line frequency) can be increased. There is, however, an interesting contradiction. Decreasing the scan velocity can also cause wear (Figure 7). The sliding velocity is an important parameter for friction forces. Sokoloff,[28] for instance, found in his model that (for sliding velocities that are small relative to the velocity of sound in the material), the friction force F_{fric} is inversely proportional to the sliding velocity v, i.e.,

$$F_{fric} = k\frac{1}{v},$$

where k is a material-specific constant. In Figure 7, the velocity-wear dependence on a mixed LB film is documented. This figure shows that wear is strongly material specific. Whereas the hydrocarbon-containing part of the film (bright islandlike structures in Figure 7a) is conspicuously modified

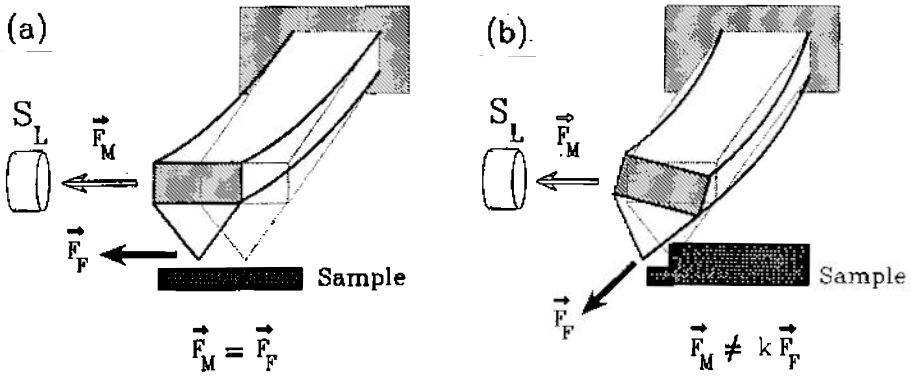

Figure 4. Lateral deflection vs. lateral measurement: (a) gliding over an atomically flat surface, and (b) gliding over a step (where k is a real constant).

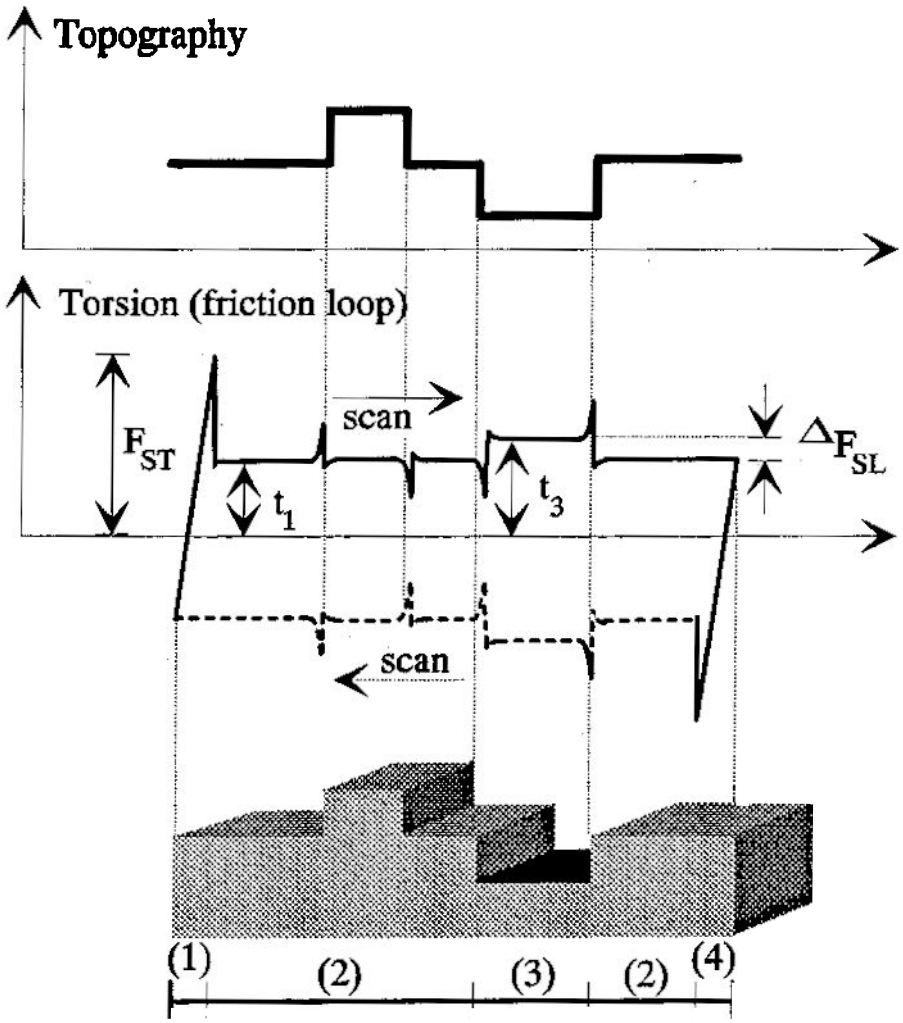

Figure 5. Friction loop and topography on a heterogeneous stepped surface. Terraces (2) and (3) are composed of different materials. In regions (1) and (4), the cantilever sticks to the sample surface because of static friction F_{ST}. The sliding friction is t_1 on part (2), and t_3 on part (3). In a torsional-force image, the contrast difference is caused by the relative sliding friction, $\Delta F_{SL} = t_1 - t_3$.

(i.e., plastically deformed), the fluorocarbon-containing part of the film (darker part of the AFM image in Figure 7a) remains defect-free at any scan velocity.

In the literature, an increase in shear strength with an increase in sliding velocity is usually observed. B.J. Briscoe and D.C.B. Evans[29] observed a proportional increase in friction force with the logarithm of the sliding velocity under constant temperature and pressure over the range of 0.3–3.4 μm/sec. Their observation agreed with a first approximation with *Eyring's model of friction*, which expresses the shear strength as a function of temperature, sliding velocity, and applied normal load. The AFM result of variable velocity cannot be explained by this theory, whereas AFM results of variable applied normal loading can be explained, in first-order approximation, as shown by our group.[30]

In the adhesive theory of friction, friction is explained by *asperity junctions*.[31] In these theories, the mechanics of stationary contact is extrapolated to the moving-contact situation. The time step of forming junctions is either infinite or zero, i.e., there is or there is not a junction. A dynamic process, however, is time dependent. Therefore, the real area of contact, A, that is formed by the asperity junctions should be time dependent, i.e.,

$$A = A(t)$$

with

$$A(t+\Delta t) > A(t);$$

and the kinetic friction F_{kin} should pass into the static friction F_{static}, i.e.

$$F_{kin}(A(t)) \xrightarrow{t \to \infty} F_{static}.$$

The above AFM result of increasing wear by decreasing the sliding velocity supports these assumptions. With this explanation, static friction could be regarded as a limiting case of kinetic friction.

Inter- and intralayer interaction can be compared on one- and two-bilayer Cd-arachidate Langmuir-Blodgett films by intentionally modifying the film surface and also by comparing the stacking behavior of two- or four-layer films. Steps in one-bilayer films are mostly one monolayer in height (~27 Å), and two-bilayer films, one bilayer in height (~54 Å) (Figure 8).

The applied force and the feedback-loop frequency required to disrupt the interfaces V_{ij} ($i = 1,2,3$ and $j = 2,3,4$), schematically represented in Figure 9, allow a ranking of the interlayer (V_{23},V_{34}) and substrate-film interaction V_{12}, which is:

$$V_{34} < V_{23} < V_{12}.$$

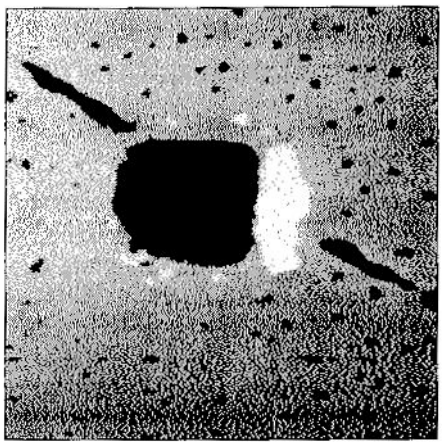

Figure 6. Intentionally created hole in a four-layer LB film. 2.5 × 2.5-μm^2 AFM image of Cd-arachidate film. A quadratic hole has been created by increasing the scan speed from 0.5 μm/sec to 5 μm/sec (the load was also increased by about a factor of 10, to 10^{-7} N). Damage was found to start at step edges where the torsion is strong. Laterally increased shear stress in the film can be observed in the vicinity of the hole, where the density of pores is decreased.

This scratching experiment corresponds to nondestructive measurements on various sample sites, which show that:

- the interaction between the polar heads, V_{23}, is stronger than the interaction between the hydrophobic tails, V_{34}. This follows from the dominance of bilayer steps in the four-layer system; and
- the substrate-film interaction, V_{12}, is the strongest of all three of the mentioned interface interactions. This statement is deduced from the phenomenon that, in the one-bilayer system, mostly monolayer steps and rarely uncovered substrates are found.

Whereas it is easy to scratch the first bilayer (counted from the film-air interface) of the two-bilayer system, it is difficult to remove the film entirely and to uncover the silicon substrate. Entire sheets are removed in the scratching process. This indicates larger intralayer interactions than interlayer interactions.

The ranking of the interactions can be estimated by the strength of the acting potentials. Attractive hydrophobic forces are acting between the tails of the molecules. They are much stronger than the van der Waals attraction at small separation and are of surprisingly long range.[23,32] Hydrophilic interactions are repulsive and form, together with the hydrophobic interactions, some nonadditive net intralayer interaction. Cd ions—surfactants at the heads of the amphiphilic molecules—have the effect of stabilizing the film.[42] The hydrophobic interaction V_{12} is expected to be very strong. Considering the length of the molecules, it seems reasonable that the intralayer interaction dominates the interlayer interaction, as concluded by the AFM results. The ranking $V_{34} < V_{23}$, however, cannot be explained by these two driving forces. It might be possible that the saponification (hydrolysis of esters into acids and alcohols) of the films that leads to the formation of strong ionic bonds is responsible. Future experiments with pure arachidic acid will clarify whether the ranking of interlayer forces is as pronounced as in the case of the soap Cd-arachidate.

Friction Measurements on Organic Lubricants

Friction measurements on

- the above-presented multilayers of Cd-arachidate LB films on silicon (for experimental details see Reference 30), and
- phase-separated LB films of mixtures of hydrocarbons and fluorocarbons on silicon

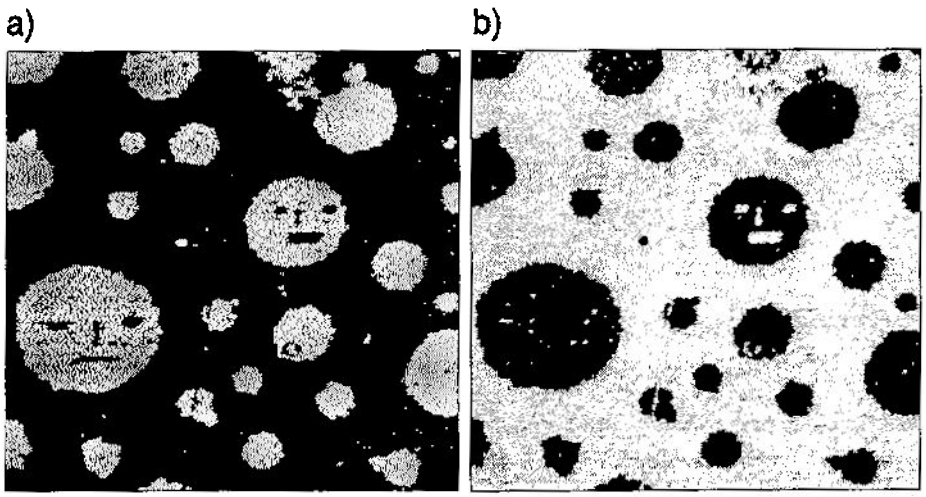

Figure 7. Structures created in mixed monolayer film by low-speed scanning: (a) 2.5 × 2.5-μm^2 AFM image of a 1:1 mixture of fluorocarbons (dark) and hydrocarbons (bright). "Smileys" were written with the AFM by decreasing the scan speed from ~1 μm/sec to 0.01 μm/sec. Under these conditions, only the islandlike structures (hydrocarbons) could be scribed by the AFM cantilever tip. The fluorocarbon-containing part of the film could not be destroyed by scan-speed reduction. (b) Friction-force map of the same region. Brighter areas have higher friction.

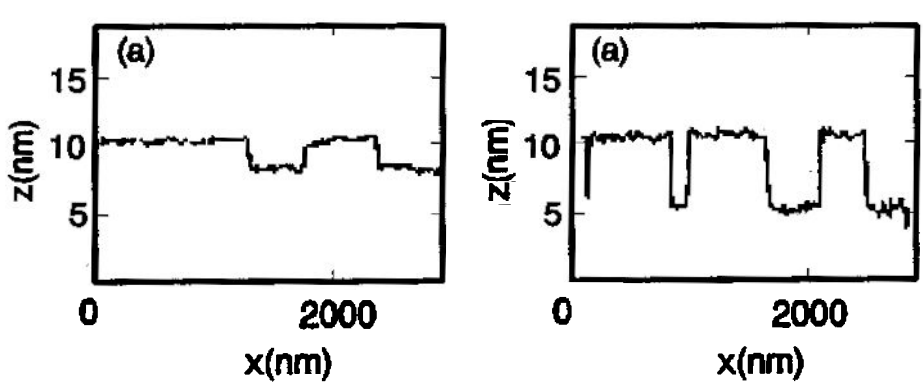

Figure 8. Line trace of the single and double bilayer films. (a) Monolayer steps in the bilayer film. (b) Mainly bilayer steps are found in the double bilayer films.

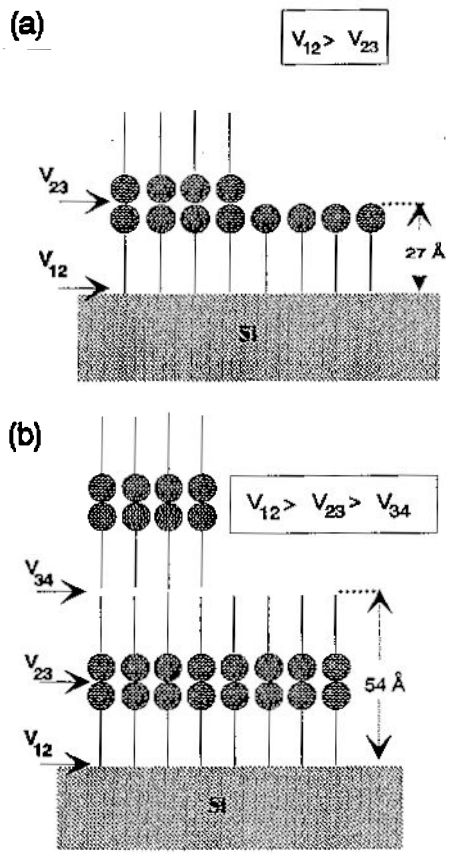

Figure 9. Schematic drawing of the stepped Cd-arachidate films: (a) one-bilayer Cd-arachidate film, and (b) two-bilayer Cd-arachidate film. The relative strength of interlayer potentials, V, are determined with the AFM (see text). The silicon substrate was hydrophobized.[33]

(for experimental details see Reference 43), provide material-specific identification. The studies were carried out on two-bilayer films on hydrophobized silicon wafers.

Figure 10a is a top-view image of a Cd-arachidate bilayer film. The image contains three different levels: The first level (1) (*dark*) is the silicon substrate, the second level (2) (*dark grey*) is the first bilayer system (step height from the substrate 54 Å), and the third level (3) (*bright*) is the second bilayer system (108 Å). In the lateral image (*friction image*), Figure 10b, there is an evident contrast difference between level (1) and the other two levels. Together with the topographical information of Figure 10a, it is obvious that the film-covered part of the sample shows decreased relative friction of one order of magnitude (Figure 10c). The friction loop (Figure 10d) indicates increased lateral forces at step sites, arising mainly from a crosstalk from topography.

The lubricating property of such organic layers is demonstrated with the AFM, and the factor of 10 difference in lubricated and unlubricated friction agrees with macroscopic-scale friction measurements.[34]

No contrast difference can be observed between the two levels of the film (first and second bilayers). Within an uncertainty of 10%, the shear strength does not depend on the thickness of these films, whether they are a two- or four-layer system. But it is expected that multilayer films of about 10 layers or more should provide differences in shearing.

Friction force measurement under variable normal forces show no functional dependence on the applied normal load (Figure 11). The investigations, however, are performed only in the range of 1–10 nN and at low speeds of less than 1 μm/s. Wear processes start at forces above a threshold of about 10 nN, primarily at film edges. The above observation of AFM-induced shear at film islands confirms the assumption[29] that wear does not evolve continuously; instead, it starts at a critical force of 10 nN. The collective motion of molecules is preferred and the size of the sheared particles is determined by the applied shear stress.

At loads of about 10 nN, before the onset of wear, increased lateral forces at step

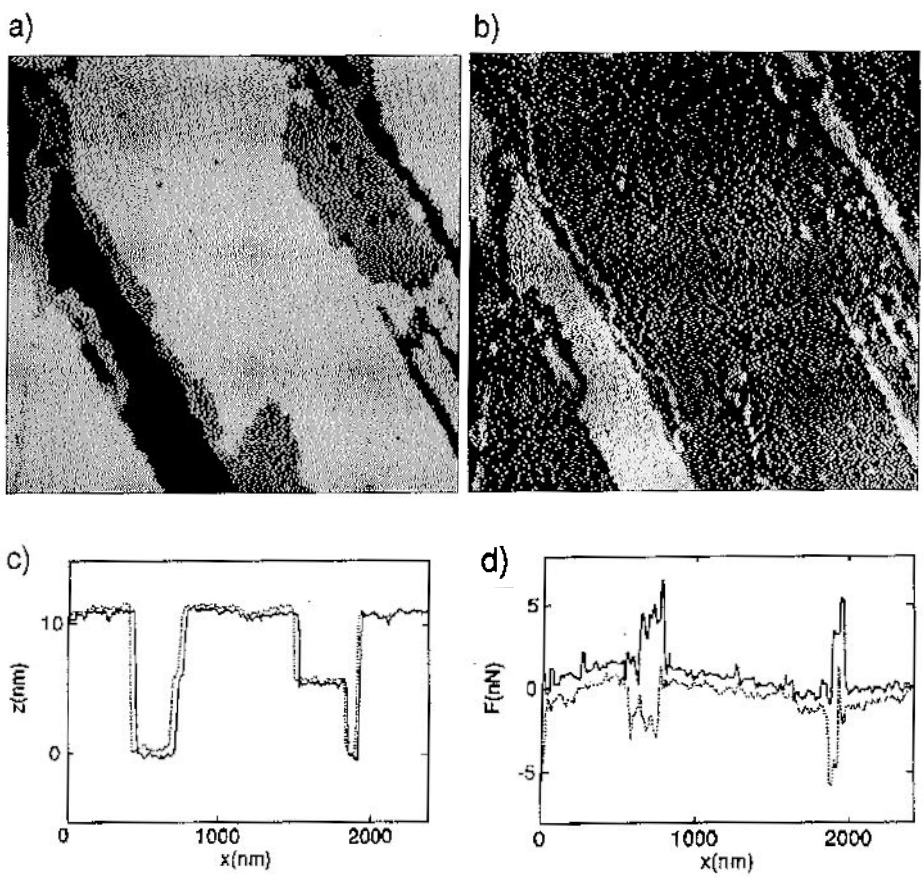

Figure 10. Bidirectional measurement of a four-layer Cd-arachidate LB film. (a) 2.0 × 2.0-μm² topographical AFM image. The silicon substrate (dark), (level 1); one-bilayer system (dark grey), (level 2); and two-bilayer system (bright), (level 3) are imaged. The step heights are 54 Å. (b) Simultaneously measured friction-force map shows increased friction (light areas) on the substrate as compared to that on the organic films. No difference in friction is measurable between single- and double-bilayer surfaces. At step sites, an increased lateral signal caused mainly by topographical crosstalk, is documented. (c) Forward (solid line) and reverse (dotted line) scan lines of topography. (d) Friction force loop, forward (solid line) and reverse (dotted line) scan lines of friction. The difference between the upper and lower curve, divided by two, yields the frictional force. The friction force of the LB-covered part is 0.2 nN, and on the uncovered silicon surface is 3 nN. Applied normal load is 3 nN.

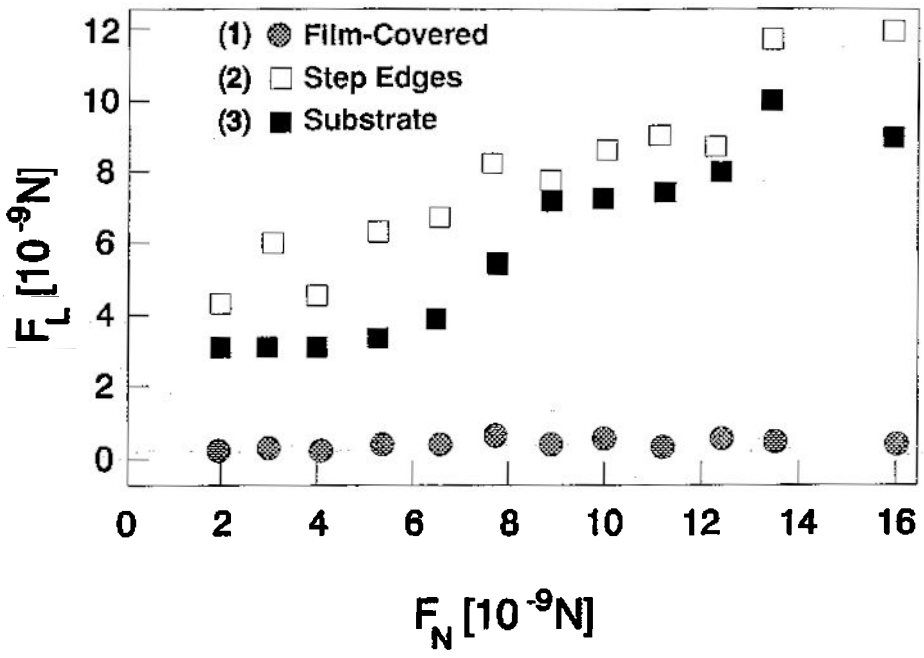

Figure 11. Lateral-force dependence on loading F_N. Lateral forces F_L are measured (1) on flat, film-covered areas, (2) at step edges, and (3) on the substrate. On film-covered areas, the lateral forces remain constant. Lateral forces on the substrates and at the step edges increase as a function of the applied normal load.

sites are measured (Figure 11). As already mentioned above, lateral forces are higher at step edges. Varying the applied normal load in the range of about 2–16 nN, the frictional forces at step sites varies between four and 12 nN. This increase in frictional resistance is due to nonideal force control at step edges (see the beginning of this section) and is also due to the increase, on impact, in contact area with the edge of the upper bilayer. On the silicon substrate, lateral force measurements increase as a function of normal forces.

Figure 12a shows a 5.0 × 5.0 μm^2 top-view AFM image of a 1:1 molar mixture of arachidic acid and partially fluorinated carboxylic acid bound ionically to a common cationic polymer (see schematic representation of the carboxylates in Figure 13). Round islandlike structures, 100 nm to 1 μm in diameter and 1.6 nm in height, above a surrounding sealike film are observed. The higher circular domains in Figure 12a are assigned to the hydrocarbons and the surrounding flat film to the fluorocarbons, based partly on their different molecular lengths and partly on their different frictional behaviors (described later in this section). With molecular lengths of ~2.5 nm and ~2.0 nm for the arachidic acid and the fluorocarbon-terminated acid, respectively, a difference in height of ~1.0 nm between domains of the two components in this bilayer LB system is anticipated. Figure 12a shows a step height from sea to island of 1.6 nm, a slightly greater difference that could be due to a greater tilt angle in the fluorocarbon domains.[35]

In a separate series of experiments, AFM images have been recorded on LB bilayer films composed of a single carboxylic acid component: one from arachidate and one from the partially fluorinated carboxylate. The fluorinated acid film contains fewer defects than the arachidic acid film. These results support the assignment of the circular domains to the hydrocarbon component, since holes are only observed in the circular domains in the mixed films. These holes are ~5.0 nm in depth, consistent with the thickness of a bilayer. Furthermore, increasing the force while scanning disrupts the hydrocarbon but not the fluorinated areas, in both the one- and two-component films. The fluorinated sites show good resistance to rupture during sliding, which is in agreement with previous tribology experiments in the literature, using macroscopic measurement techniques.[29]

Lateral-force measurements (Figure 12b) performed simultaneously with the topography measurements (Figure 12a) roughly indicate friction that is four times higher over the fluorinated regions than over the hydrocarbon regions. Holes in the film reveal the silicon substrate (Figure 12b). The silicon, appearing as bright areas of high contrast in the lateral image, displays a friction force that is a factor of ten higher than the hydrocarbon domains. This difference in friction is in good agreement with other experiments performed on both the macroscopic and nanometer scales.[26,27,36] In sum, from the AFM measurements on these phase-separated LB films, the relative friction of the hydrocarbon, fluorocarbon, and silicon surfaces are shown to be 1:4:10.

The differences in friction are not due to changes in topography. This point is demonstrated particularly well by the ability of the friction measurements to identify the scattered islands of *extraneous* material sitting atop hydrocarbon domains. Whereas by *normal*-force measurement, only the geometry of the island is determined, by *lateral*-force measurement, the composition of the island is determined. The frictional response of the island corresponds to that of the circular hydrocarbon domains, thereby allowing it to be identified as hydrocarbon in nature. This assignment would not be possible with the normal AFM alone.

A surprising result is that the friction on the fluorinated areas is higher than that on the hydrocarbons. From the performance of fluorine-containing lubricants, such as Teflon® (PTFE), a reduction in friction might be expected. However, it is known from surface force apparatus (SFA) experiments[29] that fluorinated LB films have larger shear strengths than their hydrogen-containing counterparts.

These observations of friction and robustness on the scale of nanometers can be applied to the study of tribology, particularly boundary lubrication. Boundary lubrication, as established by Hardy,[37] deals with the lubricating effect of the layers of lubricant in closest proximity to the solid surfaces undergoing frictional contact, and is of far-reaching importance in most surface-on-surface sliding mechanisms. The particular advantage of the fluorinated film is its resistance to rupture, as known from both the SFA[29] and AFM measurements. Therefore, the good performance of the fluorocarbon films as lubricants can be traced to an excellent stability in the presence of applied stress and a reduced friction (compared to unlubricated surfaces), which create a reduction in wear to low values (reduction by a factor of 10,000).[38]

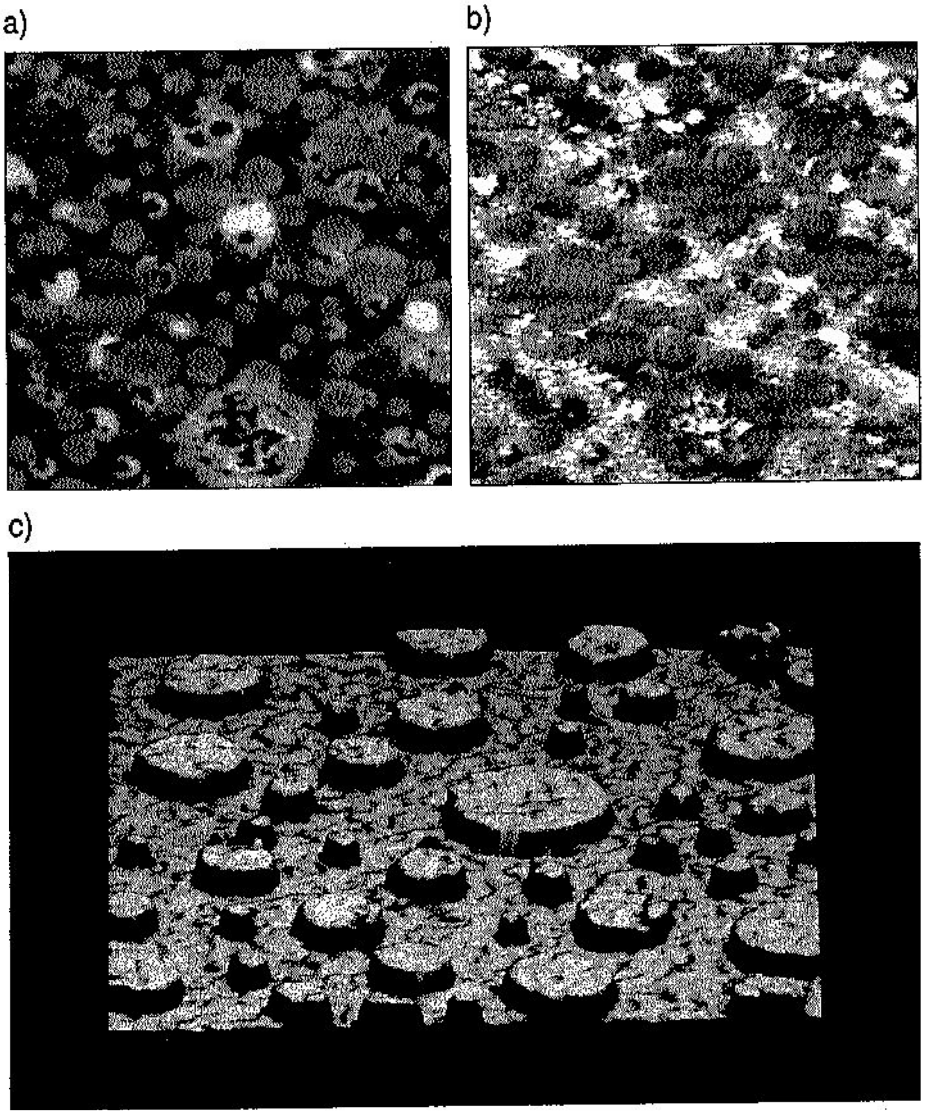

Figure 12. Simultaneous normal and friction measurements on a bilayer mixed LB film. (a) 2.5 × 2.5-μm² AFM image of the surface of the bilayer prepared from a mixture of the fluorocarbon and hydrocarbon carboxylates (1:1 molar). The image represents the topography. The circular domains are assigned to the hydrocarbon component and the surrounding flat film to the partially fluorinated component. The difference in height surrounding flat film to the partially fluorinated component. The difference in height between these two regions is ~1.6 nm. Holes of about 5 nm in depth are only observed in the islandlike circular hydrocarbon domains, whereas the fluorinated film remains fairly uniform and continuously unbroken. (b) Simulataneously measured friction-force map. The lateral-force image indicates higher friction (brighter contrast) over the fluorinated regions. Highest friction is measured on the silicon surface (at the bottom of the holes in the film). No difference in contrast (friction) is observed between the hydrocarbon layers of different heights. (c) Three-dimensional display topographical image.

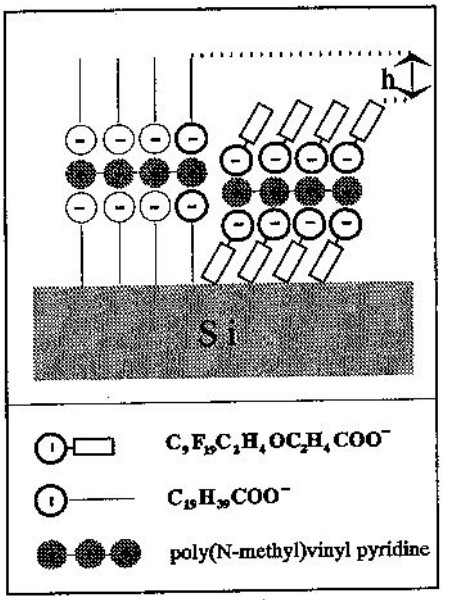

Figure 13. Schematic view of the LB bilayer system imaged by AFM in Figure 12. The h represents the height difference of ~1.6 nm between the hydrocarbon and fluorocarbon species (see text).

Conclusions

The AFM is well-suited for studying wear and frictional behavior by simultaneous, bidirectional normal and lateral measurements. It has been shown that complex phenomena of boundary lubrication can be studied. Material-distinct identification can be performed and film inhomogeneities exposed. Wear studies on LB films reveal an interesting functional behavior depending on sliding velocities. This new technique allows a variety of tribological studies on all kind of materials, for example, inorganic compounds, that are most likely investigated under ultrahigh vacuum conditions to avoid ambient film formation on the surface;[9,18] the origin of the resistance to sliding, such as elastic properties of the materials;[13] and interaction forces.[39]

Acknowledgments

We wish to thank J. Frommer for helpful and stimulating discussions and M. Fujihira for the preparation of some of the samples and very fruitful discussions. This work was supported by the Swiss National Science Foundation and the Kommission zur Förderung der wissenschaftlichen Forschung.

References

1. G. Binnig, C.F. Quate, and C. Gerber, *Phys. Rev. Lett.* **56** (1986) p. 930.

2. For recent reviews of scanning force microscopies, see: E. Meyer and H. Heinzelmann, *Scanning Tunneling Microscopy and Related Methods*, edited by R.J. Behm (Kluwer, Dordrecht, 1990) p. 443; J. Frommer and E. Meyer, *J. Phys. Cond. Matt.* **3** (1991) p. S1; *Ultramicroscopy* **42–4** (entire volumes devoted to scanning tunneling microscopy and scanning force microscopies) (1992); W. Heckl, *Thin Solid Films* **210–211** (1992) p. 640; and J. Frommer, *Angewandte Chemie*, Int. Ed. Engl. **31** (1992) p. 1298.
3. G. Binnig and H. Rohrer, *Helv. Phys. Acta* **55** (1982) p. 726; and G. Binning, H. Rohrer, Ch. Gerber, and E. Weibel, *Phys. Rev. Lett.* **49** (1982) p. 57.
4. C.M. Mate, G.M. McClelland, R. Erlandsson, and S. Chiang, *Phys. Rev. Lett.* **59** (1987) p. 1942.
5. G. Meyer and N.M. Amer, *Appl. Phys. Lett.* **57** (1990) p. 2089.
6. O. Marti, J. Colchero, and J. Mlynek, *Nanotechnol.* **1** (1990) p. 141.
7. R. Erlandsson, G.M. McClelland, C.M. Mate, and S. Chiang, *J. Vac. Sci. Technol. A.* **6** (1988) p. 266.
8. G. Neubauer, S.R. Cohen, G.M. McClelland, D. Horne, and C.M. Mate, *Rev. Sci. Instrum.* **61** (1990) p. 2296.
9. G.M. McClelland, *Adhesion and Friction*, edited by M. Grunze and H.J. Kreuzer (Kluwer, Amsterdam, 1992) p. 81.
10. G. Meyer and N.M. Amer, *Appl. Phys. Lett.* **57** (1990) p. 2089.
11. O. Marti, J. Colchero, and J. Mlynek, *Nanotechnol.* **1** (1990) p. 141.
12. R.M. Overney and E. Meyer (private communication).
13. R.M. Overney, PhD thesis, University of Basel, 1992.
14. Park Scientific Instruments, 1171 Borregas Avenue, Sunnyvale, CA 94089.
15. O. Wolter, T. Bayer, and J. Grechner, *J. Vac. Sci. Technol. B* **9** (1991) p. 1353; O. Wolter, Institut für Mikrostrukturtechnik und Optoelektronik, Wetzler Blankenfeld/Germany.
16. K.E. Petersen, "Silicon as a Mechanical Material," *Proc. IEEE* **40** (1982) p. 420.
17. E. Meyer, R. Overney, R. Lüthi, D. Brodbeck, L. Howald, J. Frommer, and H-J. Güntherodt, *Thin Solid Films* **220** (1992) p. 132.
18. L. Howard, E. Meyer, R. Lüthi, H. Haefke, R. Overney, H. Rudin, and H-J. Güntherodt, submitted to *Applied Phys. Lett.* (1993).
19. S.M. Hsu, *MRS Bulletin* XVI (10) (1991) p. 54.
20. For recent reviews of thin organic films, see: A. Ulman, *An Introduction to Ultrathin Organic Films, From Langmuir-Blodgett to Self-Assembly* (Academic Press, San Diego 1991); and J. Swalen, *Annual Rev. Mater. Sci.* **21** (1991) p. 373.
21. R.M. Overney, E. Meyer, J. Frommer, H-J. Güntherodt, G. Decher, J. Reibel, and U. Sohling, *Langmuir* **9** (1992) p. 341.
22. E. Meyer, L. Howald, R. Overney, H. Heinzelmann, J. Frommer, H-J. Güntherodt, T. Wagner, H. Schier, and S. Roth, *Nature* **349** (1991) p. 398.
23. R. Overney, E. Meyer, J. Frommer, D. Brodbeck, R. Lüthi, L. Howald, H-J. Güntherodt, M. Fujihira, H. Takano, and Y. Gotoh, *Nature* **359** (1992) p. 349; and E. Meyer, R. Overney, R. Lüthi, D. Brodbeck, L. Howald, J. Frommer, H-J. Güntherodt, O. Wolter, M. Fujihira, H. Takano, and Y. Gotoh, *Thin Solid Films* **220** (1992) p. 132.
24. L. Bourdieu, P. Silberzan, and D. Chatenay, *Phys. Rev. Lett.* **6** (1991) p. 2029; and C. Alves, E. Smith, and M. Porter, *J. Amer. Chem. Soc.* **114** (1992) p. 1222.
25. H. Fuchs, L. Chi, L. Eng, and K. Graf, *Thin Solid Films* **210–211** (1992) p. 655.
26. E. Meyer, L. Howald, R. Overney, H. Heinzelmann, J. Frommer, H.-J. Güntherodt, *Ultramicroscopy* **42–44** (1992) p. 274.
27. E. Meyer, R. Overney, L. Howald, D. Brodbeck, R. Lüthi, and H-J. Güntherodt, *Fundamentals of Friction*, edited by I. Singer and H. Pollock (Kluwer, Dordrecht, 1992) p. 427.
28. J.B. Sokoloff, *Phys. Rev B* **42** (1990) p. 760.
29. B.J. Briscoe and D.C.B. Evans, *Proc. R. Soc. London, Ser. A* **380** (1982) p. 389.
30. E. Meyer, R. Overney, D. Brodbeck, L. Howald, R. Lüthi, J. Frommer, and H-J. Güntherodt, *Phys. Rev. Lett.* **69** (1992) p. 1777.
31. F.P. Bowden and D. Tabor, *Friction and Lubrication of Solids*, Part 1 (Clarendon Press, Oxford, 1954).
32. J.N. Israelachvili, *Intermolecular and Surface Forces*, 2nd ed. (Academic Press, London, 1991).
33. M. Schreck, D. Schmeisser, W. Göpel, H. Schier, H.U. Habermeier, S. Roth, and L. Dulog, *Thin Solid Films* **175** (1989) p. 95.
34. A.J. Bailey and J.S. Courtney-Pratt, *Proc. R. Soc. London, Ser. A* **227** (1955) p. 501.
35. C. Naselli, J.D. Swalen, and J.F. Rabolt, *J. Chem. Phys.* **90** (1989) p. 3855.
36. B. Briscoe, D. Tabor, *Interfacial Phenomena in Apolar Media*, edited by H-F. Eicke, G.D. Parfitt (Marcel Dekker, New York, 1987) p. 327.
37. W.B. Hardy, *Proc. R. Soc. London, Ser. A* **88** (1913) p. 313.
38. E. Rabinowitz, D. Tabor, *Proc. R. Soc. London, Ser. A* **208** (1951) p. 455.
39. A. Wadas and R.M. Overney (private communication).
40. J.N. Israelachvili and D. Tabor, *Proc. R. Soc. London, Ser. A* **331** (1972) p. 19.
41. D. Dowson, *History of Tribology* (Longman, London, 1979).
42. E. Meyer, R. Overney, R. Lüthi, D. Brodbeck, L. Howard, J. Frommer, H-J. Güntherodt, O. Wolter, M. Fujihira, H. Takano, and Y. Gotoh, *Thin Solid Films* **220** (1992) p. 132.
43. R. Overney, E. Meyer, J. Frommer, D. Brodbeck, R. Lüthi, L. Howard, H-J. Güntherodt, M. Fujihira, H. Takano, and Y. Gotoh, *Nature* **359** (1992) p. 349. □